Study of Adhesion Recovery phenomenon using a Multi-axle Roller-rig

(Article begins on next page)

03 May 2024

PAPER • OPEN ACCESS

Study of Adhesion Recovery phenomenon using a Multi-axle Roller-rig

View the article online for updates and enhancements.

Study of Adhesion Recovery phenomenon using a Multi-axle Roller-rig

Matteo Magelli

Department of Mechanical and Aerospace Engineering, Politecnico di Torino, Corso Duca degli Abruzzi Corso Duca degli Abruzzi, 24, 10129, Torino, Italy

matteo.magelli@polito.it

Abstract. When a railway vehicle is running on a contaminated track, the available friction is reduced, and large creep values arise at the wheel-rail interface. However, the work of the friction forces of the leading wheelsets produces a cleaning effect on both the track and the wheels, so that the contaminant layer is partially removed, and adhesion increases on the leading as well as on the trailing wheelsets. The investigation of these adhesion recovery phenomena is the key to develop new solutions aiming to improve the vehicle dynamic behaviour in degraded adhesion conditions. Since on-field tests are usually expensive and time-consuming, roller-rigs are the typical apparatus used to simulate the vehicle dynamic behaviour in laboratory conditions. The paper describes the mechanical design of an innovative roller rig specifically designed to study adhesion recovery phenomena, consisting of four wheelsets running over the same pair of rollers. Experimental tests are performed on the test bench to obtain adhesion characteristics under dry and contaminated conditions.

1. Introduction

Due to the possible presence of contaminant layers on the track, the wheel-rail friction coefficient can significantly decrease with respect to dry adhesion condition values, with a negative impact on safety, wheel profile wear and traction/braking performances. Both natural and artificial substances can be lying at the wheel-rail contact patch. Natural substances lying on the rails include water [1-3] due to morning dew and rain, as well as autumn leaves [4-6], but also oxides, dust, etc. [7,8]. Artificial substances are products intentionally spread at the wheel-rail interface to control and manage adhesion and contact conditions. Originally, sand [9-13] was spread on the rails to restore dry adhesion values in case of wet or leaf contaminated rails, however sand particles can lead to a big increase of the abrasive wear of wheel and rail surfaces. In the last decades, engineered products, named friction modifiers (FMs), have been studied and developed in both solid and liquid form, with the aim to guarantee a constant wheel-rail friction coefficient at a best compromise value in terms of traction/braking performance, rolling noise, rolling contact fatigue (RCF), wear of wheel and rail surfaces, energy consumption, etc. [14-19]. Furthermore, the wheel tread–rail head interface can be accidentally contaminated by oil [20] or grease [21] that are intentionally spread at the wheel flange–rail gauge interface in sharp curves to reduce wear.

Despite sand and FM spreading being the most common methods to ensure good adhesion conditions, modern vehicles are also fitted with wheel slide protection (WSP) [22,23] and antiskid [24-26] systems, i.e., mechatronic devices controlling the braking and tractive efforts respectively, in order to fully exploit the available friction in any contact condition. These systems usually aim to take

advantage of the linear stable part of the adhesion curve, corresponding to an adhesion increasing trend with increasing creep.

Although these mechatronic devices are embedded with performing algorithms [27,28] which do avoid full sliding conditions and consequent wear of the wheel surfaces, they do not commonly consider the cleaning effect of the friction forces at large creep values, which can lead to a big adhesion recovery. In fact, when large creepage values are generated on a wheelset running under degraded adhesion conditions, the work of the friction forces can partially remove the contaminant layer from the wheels (wheel adhesion recovery) and from the rails (rail adhesion recovery). In the latter case, the leading wheelsets reduce the contaminant film thickness so that the trailing wheelsets can run on the same track section with a higher coefficient of friction. Therefore, the effectiveness of the WSP and antiskid algorithms could be drastically improved considering the adhesion recovery phenomenon and the mutual influence among all the wheelsets in the vehicle configuration.

Proper working of mechatronic system algorithms clearly relies on the implemented adhesion models, which calculate adhesion as a function of creepage and contact conditions. Classical models, such as Kalker's exact theory CONTACT [29], the Fastsim [30] simplified algorithm and the heuristic model proposed by Shen et al. [31], are typically valid for dry adhesion conditions. Therefore, they do not produce completely reliable results in degraded adhesion conditions when large creep values exist at the wheel-rail interface.

More recently, some models have been proposed considering the falling friction effect, i.e., the reduction of friction coefficient with increasing sliding speed, and the reduction of the friction coefficient due to the contaminant layer lying on the track, which usually leads to a reduction of the initial slope of the adhesion curve in the stable part. Among these models are Polach's global contact model [32,33], the heuristic model from Politecnico di Torino [34], a modified version of CONTACT, developed by Vollebregt [35] and an extended Fastsim algorithm, as an outcome of a collaboration between Polach and the Central Queensland University railway research group [36]. Polach's global contact model is computationally efficient, and it is widely used in many multibody software packages (MBS), while the modified CONTACT tool is typically too time-consuming for quick vehicle dynamic simulations. The Politecnico di Torino model has the big advantage of low computational times due to the closed form of all the equations, including the expression for the falling friction. The extended Fastsim algorithm is computationally slower with respect to Polach and Politecnico di Torino global contact models, however it is a local model which allows to calculate the tangential stresses and sliding velocities in each cell of the discretized contact patch. For this reason, local contact models, which compute the tangential pressure distribution on the contact patch, are usually adopted for wear and tribological studies [37].

Although these recent models allow to consider the friction reduction due to contaminants and the falling friction effect, they do not take into account the cleaning effect of the friction forces and the adhesion recovery caused by large creep values. Therefore, some work has been carried out in the last few years to develop new innovative models including the variation of the friction conditions related to the reduction of the contaminant layer thickness due to large creep and dissipated power values. The Italian railway research team from Università degli Studi di Firenze [38] tried to simulate the wheel adhesion recovery phenomenon using the heuristic law suggested by Shen et al. including a new reduction factor, different in forward, i.e., increasing creep, and backward, i.e., decreasing creep, conditions. The new reduction factor is a function of both the creep and its time derivative. Then, the same research team developed a new model admitting that the adhesion coefficient value is limited by an upper curve, related to full adhesion recovery conditions, and a lower curve, corresponding to degraded adhesion conditions [39]. The switch between the two curves, which are mathematically described according to Polach's model, is managed by means of a smoothing transition exponential law, including a model tuning parameter. This global model was recently upgraded and the degraded adhesion equations were applied locally in Fastsim, in order to obtain different values of the adhesion coefficient on the contact patch, so as to develop a local degraded adhesion model [40].

The main drawback of these models is that they were all tuned and validated on experimental data collected from full-vehicle tests performed on a UIC-Z1 coach in Velim by Trenitalia. However, on-track tests [41] are usually extremely expensive and time consuming. Moreover, they lack good reproducibility of test conditions and they are strongly influenced by the specific design parameters of the tested vehicle. Therefore, a good compromise solution widely adopted in the railway field to collect data on wheel-rail contact and adhesion is using laboratory devices, mainly twin-disc systems [12,42,43] and full-scale or scaled roller-rigs [44-48]. Roller-rigs can guarantee a good reproduction of the vehicle dynamics, however differences exist between the wheel-rail and the wheel-roller contacts, which should be accounted for during laboratory activities [49-51].

Voltr and Lata [52,53] used a full-scale single wheel roller-rig to investigate the adhesion recovery phenomenon in traction conditions, consisting of a powered roller, controlled in speed, and a powered tram wheel, controlled in torque mode, thus superimposing large creep values in traction conditions. The authors identified different adhesion behaviors according to the maximum creepage value reached in the experimental tests, and they also tried to model the phenomenon with a strategy similar to the one proposed by the Università degli Studi di Firenze researchers, by assuming that the adhesion coefficient falls between two Polach curves, featuring two separate values of the static coefficient of friction. The variation of the static coefficient of friction is assumed to be proportional to the specific dissipated work in a limited time interval, i.e., a model parameter called "memory". Moreover, the hysteretic loop observed in adhesion recovery tests is reproduced by including a term proportional to the derivative of the sliding speed, with positive and negative values in forward and backward directions, respectively. Although this test campaign provided a huge amount of significant experimental data, the test stand used by Voltr and Lata only allows for the simulation of the wheel adhesion recovery, while the rail adhesion recovery phenomenon cannot be investigated, since the bench simply includes a single wheel running over a roller.

Researchers from Politecnico di Torino [54] tried to replicate in laboratory conditions the rail adhesion recovery phenomenon by means of a single wheelset 1:5 scaled roller rig equipped with a contaminant probe and a cleaning system, with the aim to replicate the passage of many wheelsets on the same track section. The cleaning system aimed to reduce the contaminant layer thickness, reproducing the effect of the leading wheelsets on a real vehicle. Although good results were obtained in the tests, the authors declared that the success of the experiments was significantly dependent on the proper working of both the cleaning system and the probe, while defects in these systems could lead to a difficult understanding of the collected data. Therefore, the research team decided to design a new innovative test bench consisting of four wheelsets acting over the same roller pair, called multi-axle roller rig, so that the real situation of consecutive wheelsets running over the same track section could be simulated with a greater accuracy [55-57].

The paper deals with the demonstration of the feasibility of the investigation of wheel as well as rail adhesion recovery phenomena by means of the new multi-axle test bench, which differs from the typical roller-rig configuration in having four wheelsets running over the same pair of rollers, thus simulating the real condition of a vehicle with many wheelsets running over the same track surface. Moreover, the creep value at the wheel-roller interface is adjusted by means of a braking system, so that transient braking operations can be simulated on the bench instead of steady-state traction maneuvers.

The first section of the paper deals with a brief description of the bench mechanical configuration and sensor arrangement, as well as of the bench control strategy. Then, attention is drawn to the three kinds of experimental tests that the bench allows to perform, namely simple adhesion curve tests, wheel adhesion recovery tests and finally rail adhesion recovery tests. The third section concerns the preliminary experimental results obtained on the bench in wheel and rail adhesion recovery tests. For the wheel adhesion recovery tests, the experimental forward and backward curves are fitted with Polach equations, and a discussion on the variation of the main model parameters due to the adhesion recovery phenomenon is carried out. Finally, some conclusions summarizing the main innovation of

the presented test bench and the preliminary results acquired in wheel and rail adhesion recovery tests are given.

2. The multi-axle roller-rig

The multi-axle roller-rig was specifically designed by the research team from Politecnico di Torino to investigate the adhesion recovery phenomenon, considering the mutual influence among all the wheelsets composing the railway vehicle. In fact, the main novelty of the new test bench with respect to typical scaled roller-rig is that it includes four wheelsets installed over the same roller pair, so that the real situation of a vehicle with all its wheelsets running over the same track section can be better simulated. The new bench is a 1:5 scaled roller-rig, which follows the Jaschinksi's similitude rule [48,58], ensuring that the acceleration of the real and scaled systems are equal to each other.

The bench, shown in Figure 1, is built with the following main modular elements:

- A main frame.
- Two rollers, powered by a 6-pole AC brushless motor, having an integral rotation thanks to a mechanical joint.
- Four wheelsets, each one provided with two brake discs and two axle-boxes.
- A pneumatic braking system consisting of two brake disc-brake caliper pairs installed on each wheelset, to allow an independent braking effort on each wheelset.
- A suspension system for each axle-box, comprising an adjustable spring element to set the value of the normal load acting at the wheel-roller contact and to compensate for the different angular displacements of the four wheelsets.
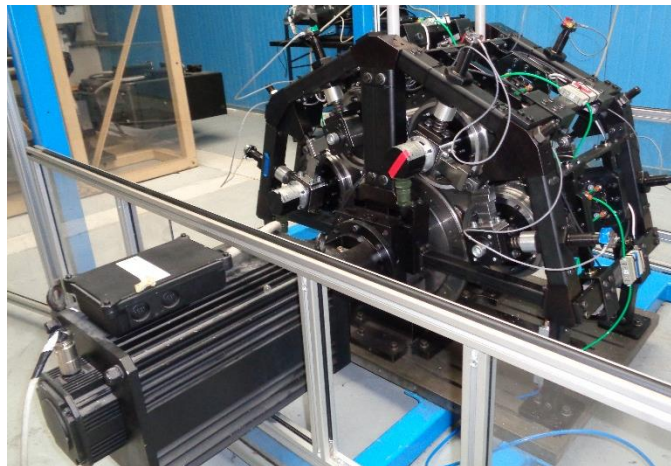

Figure 1. The multi-axle roller-rig.

Both the rollers and the wheels are made up of a hub and a rim. The external surface of the roller rim replicates the UIC60 rail profile canted 1:20, while the wheel rim is machined to the S1002 wheel profile. The longitudinal and lateral position of each wheelset can be independently adjusted and then rigidly fixed to the main frame, while the normal load acting at each wheel-roller contact patch is adjusted by means of the suspension system.

The big advantage of the modular design of the multi-axle roller-rig is that with few changes to the mechanical arrangement of the bench described in this paper, the test rig can be used to validate on-board monitoring systems for the air brake plant [59], simulating a transient braking operation of a freight vehicle [60].

The creepage value between the peripheral speed of each wheelset and the peripheral speed of the rollers can be independently adjusted by modifying the braking pressure on each wheelset. Therefore, the creepage conditions reproduced on the bench correspond to braking maneuvers, so that the new test bench allows to perform dynamic analyses and to obtain adhesion curves in transient conditions. The research group had already developed a similar arrangement for the simulation of braking

operations on roller-rigs in a previous activity performed on a single wheelset scaled roller rig [61]. This is a big difference with respect to other typical configurations of twin-disc systems and roller-rigs witnessed in the literature, which include powered rollers and powered wheelsets in order to superimpose steady-state creepage conditions, with creepage values corresponding to traction operations. In all experimental tests, which are deeply shown in the next section, the roller speed is kept constant and two different control modes can be performed, i.e., torque and speed control modes. Adhesion curves obtained during the bench calibration stage proved to be independent from the control mode, at least on a first approximation, [62], however tests shown in the paper were performed in torque control mode, which is more robust at low speed.

The roller-rig also includes transducers to measure the quantities of interest during the experimental tests. All the measured signals are acquired by acquisition cards, while the bench control and management is performed with an industrial PC through a dedicated software developed in LabVIEW 2016. The software relies on queues and it allows to acquire all signals from the acquisition cards at a rate of 1 kHz. Figure 2 gives a schematic view of the test bench data acquisition strategy.

Each wheelset is provided with an incremental encoder (1024 pulses/rev) to measure the angular displacements, which are acquired by means of a digital I/O acquisition card, applying a X4 quadrature. The numerical differentiation of this signal, performed in the post-processing Matlab routine, allows to compute the rotational speed of the wheelsets. On the other hand, the roller-speed is obtained directly from the motor drive through the Modbus/TCP IP protocol at a rate of 250 Hz. All suspension systems are fitted with a button load cell (maximum load of 1000 lb and resolution equal to 0.5 lb) measuring the normal load acting at the wheel-roller contact patch. The tangential load acting on each brake disc-brake caliper pair is measured by an S-beam cell (maximum load of 300 lb and resolution equal to 0.15 lb), so that in the post-processing stage, the wheel-roller longitudinal contact force can be calculated from the wheelset inertia and from the braking forces. The 8 normal load signals and the 8 braking force signals are acquired through two 8-channel strain bridge analog input cards. Finally, each wheelset is provided with an electro-pneumatic regulator, so that the desired value of braking pressure can be set through an USB analog output card in the range 0-9 bar. Moreover, the four valves also provide the feedback (f\b) pressure value as an output, which is acquired by means of an USB analog input module.
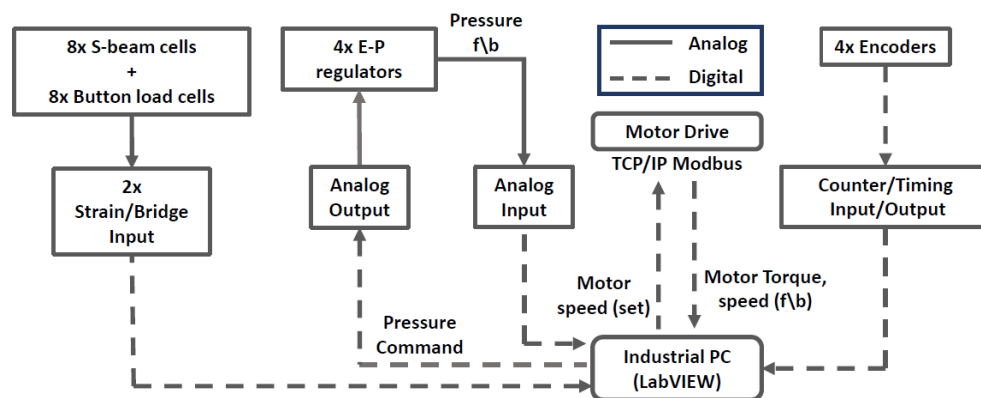

Figure 2. Schematic view of the test bench control strategy.

All the input signals as well as the motor speed and torque are saved in text files and then a post-processing routine is run in Matlab environment to filter and manage the raw data. The creepage value on the braked wheelset can be calculated from the roller and wheelset speed (ω_r and ω_w, respectively) according to equation 1, while the adhesion coefficient f is calculated as the ratio between the longitudinal contact force F_x and the normal contact force F_z, see equation 2. The normal contact force is directly obtained from the signals of the two load-button cells installed on the braked wheelsets ($F_{z,1}$ and $F_{z,2}$), see equation 3, while the longitudinal contact force is calculated from the measurements of the S-beam button cells ($F_{b,1}$ and $F_{b,2}$) by means of a rotation equilibrium equation written for the

braked wheelset, see equation 4. In equations 1-4, τ_{real} is the real transmission ratio between the wheel and the roller, experimentally determined equal to 2.006, the subscripts 1 and 2 refer to the left and right sides of the bench, respectively, r_b is the braking radius, experimentally calculated in the bench setup stage for each wheelset, I_{yy} is the wheelset polar inertia, calculated from the bench CAD model equal to 0.051 kg·m^2, d_w is the wheel diameter, equal to 0.184 m and finally $\dot{\omega}_w$ is the wheelset deceleration. The wheelset deceleration cannot be neglected on the multi-axle roller-rig since the braking system allows to perform transient braking operation instead of reaching steady-state conditions. If the wheelset deceleration is neglected, the adhesion coefficient can be significantly overestimated, especially in the nonlinear part of the adhesion characteristic.

$$\xi = 1 - \frac{\omega_w}{\tau_{real}\omega_r} \tag{1}$$

$$f = \frac{F_x}{F_z} \tag{2}$$

$$F_z = 2 \cdot \min\{F_{z,1}, F_{z,2}\} \tag{3}$$

$$F_x = \frac{2\left[r_b\left(F_{b,1} + F_{b,2}\right) - I_{yy}\dot{\omega}_w\right]}{d_w} \tag{4}$$

3. Experimental tests

The new scaled multi-axle roller-rig allows the user to perform three different experimental tests which can be selected by setting proper values of some Boolean variables in the LabVIEW bench control software. The first kind of test allows to obtain an adhesion curve just like with other scaled devices witnessed in the literature, although the new bench simulates transient braking manoeuvres rather than steady-state traction operations. Therefore, the test is carried out by increasing the braking pressure with a linear ramp until full sliding conditions are detected and a quick release signal is immediately provided to reduce the wheel and roller wear.

The second test is a wheel adhesion recovery test, which allows to obtain a hysteretic adhesion curve, comprising two separate trends corresponding to creep increasing (forward) and decreasing (backwards) ramps. The test is carried out by setting an increasing pressure ramp until a previously determined limit creepage value is obtained, and then a pressure decreasing ramp, with the same slope as the increasing one, is set until full release of the braking valve.

Both the adhesion curve and the wheel adhesion recovery tests can be performed under dry or contaminated contact conditions, however in case the hysteresis test is carried out with no interface contamination, the adhesion recovery will not be much noticeable since there is no contaminant layer to be destroyed by the friction forces, apart from little wear debris and dust or oxides. In this kind of tests, the possible contamination is to be applied when no braking effort is applied. Furthermore, the adhesion curve test can be performed by slowing down either one axle at a time or all wheelsets altogether, while the wheel adhesion recovery test requires to brake one single axle while all others keep low values of creepage during the test.

Finally, the third experimental test that the multi-axle roller rig allows to perform is the rail adhesion recovery phenomenon. Since the aim of this test is to observe the mutual influence among the four wheelsets when large creep values are generated on the contact patch, this kind of test is carried out by setting the braking pressure on all wheelsets at a constant value which ensures good adhesion levels in dry conditions. During the test, contamination is applied for a few seconds and then the rail adhesion recovery can be observed and the different adhesion levels on the four wheelsets can be recorded.

Figure 3 shows a schematic view of the three tests, considering a continuous contamination on the roller for the hysteresis curve test, while Figure 4 shows the pressure ramps used in the three tests. A big advantage of the configuration of the multi-axle roller-rig is that it allows to perform separate tests for the investigation of the wheel and rail adhesion recovery phenomena, which are usually difficult to distinguish in typical on-track operations.

The next section will deal with the presentation of the results obtained from wheel and rail adhesion recovery tests, which are related to the phenomena the bench was specifically designed to investigate. Simple adhesion curves were obtained during the bench calibration and can be found in [57,62].
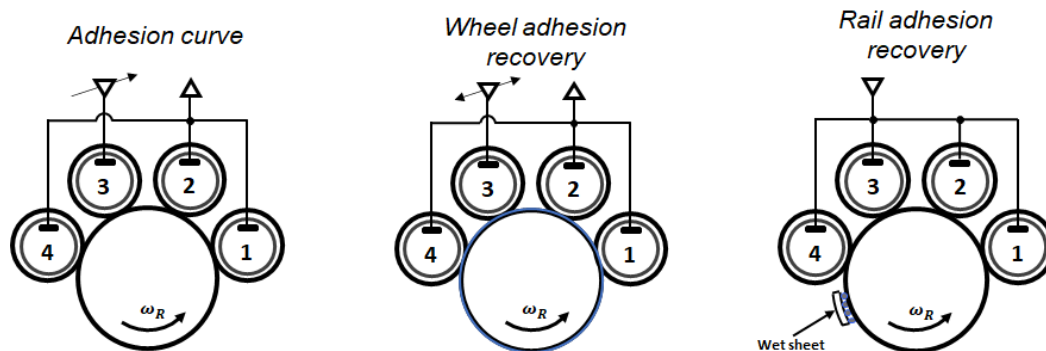

Figure 3. Experimental tests that can be performed on the multi-axle roller-rig.
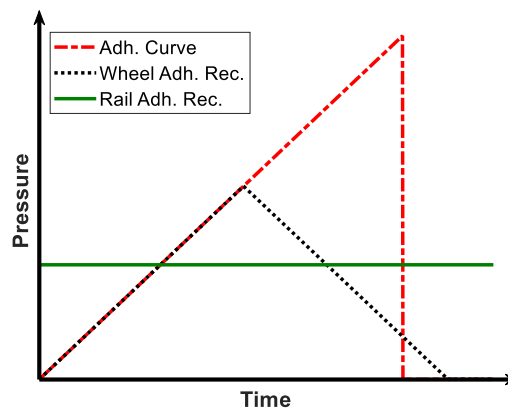

Figure 4. Pressure signals for the three tests that can be performed on the multi-axle roller-rig.

4. Results

4.1. Wheel adhesion recovery tests

This section deals with the results of the wheel and rail adhesion recovery experimental tests performed on the innovative scaled multi-axle roller-rig. The wheel adhesion recovery tests were carried out in both dry and wet adhesion conditions. Wet conditions were reproduced by manually contaminating the external surface of the two rollers with water, using a wet sheet, prior to the application of a braking pressure to the tested wheelset, so that a quite stable film of water could be formed on the roller. Tests in dry conditions did not allow to clearly highlight the adhesion recovery phenomenon since in dry conditions there is no contaminant layer to be destroyed. Therefore, in the following lines focus is only given to tests carried out simulating wet conditions.

Three values of the roller speed were considered in the tests, i.e., 100, 200 and 300 rpm, which correspond to full scale vehicle speeds equal to 15, 30 and 45 km/h, respectively. Previous works dealt with the presentation of the experimental results, however in this paper, a numerical fitting of the data is performed using the Polach model, for both forward and backwards curves.

The Polach model accounts for the falling friction effect by means of an exponential law, see equations 5-6, in which μ_0 is the static coefficient of friction, V_s is the sliding speed and B is a model parameter, related to the decrease rate of friction with increasing speed. The total contact force F can be calculated as a function of the gradient of the tangential stresses in the adhesion area ε according to

equation 7, where k_A and k_S are the reduction coefficients in the area of adhesion and slip, respectively.

$$\mu = \mu_0[(1-A)e^{-BV_s} + A] \tag{5}$$

$$A = \frac{\mu_\infty}{\mu_0} \tag{6}$$

$$F = \frac{2\mu F_z}{\pi}\left(\frac{k_A\varepsilon}{1+(k_A\varepsilon)^2} + \tan^{-1}k_S\varepsilon\right) \tag{7}$$

The gradient ε is obtained from the total creep s_{tot}, a function of the current values of longitudinal and lateral creepage as well as of the current value of spin, according to equation 8, in which C_{el} is the contact elasticity of the bodies, which can be estimated according to Kalker's equations, while a and b are the semi-axes of the contact ellipse, calculated according to the Hertzian method.

$$\varepsilon = \frac{2C_{el}\pi a^2 b}{3\mu F_z}s_{tot} \tag{8}$$

The longitudinal contact force is calculated by means of equation 9, where ξ is the longitudinal creepage:

$$F_x = F\frac{\xi}{s_{tot}} \tag{9}$$

In the fitting routine, the longitudinal creepage is known from the experimental data collected during the tests, the lateral creepage is assumed as null and the spin creepage φ is calculated as a function of the longitudinal diameters of the wheelset and the roller and of the cant angle γ, equal to 1/20, see equation 10.

$$\varphi = \gamma\frac{d_r+d_w}{d_r} \tag{10}$$

The experimental normal and longitudinal contact forces acting during the tests are computed starting from the experimental measurements performed by the button-load and S-beam cells, as previously shown in equations 3-4. The semi-axes a and b of the contact ellipse are calculated according to the Hertz theory, assuming that the lateral curvatures of the wheel and the roller are equal to the lateral curvatures of the real wheel and rail at the rolling circle (0.32 and 0.30 m, respectively), scaled by a 1:5 factor. The experimental data collected during the tests allow to obtain an adhesion curve valid for the whole axle, however, the calculation of the wheel-roller contact ellipse semi-axes in the fitting routine must be carried out considering a half of the total normal load obtained from equation (3). The calculated longitudinal contact force must thus be multiplied by 2 to obtain an adhesion characteristic for the whole wheelset. The elasticity term C_{el} is calculated with Kalker's equations.

Therefore, the model fitting routine is a least-square routine searching for the model parameters μ_0, A, B, k_A and k_S which minimize the sum of squares error (SSE) between the experimental values of the longitudinal force $F_{x,exp}$ and the longitudinal force calculated with Polach model $F_{x,model}$, see equation 11, in which N_{obs} is the total number of recorded points during the selected test. The optimization is carried out using the fmincon function in Matlab, using the default interior-point algorithm [63,64].

$$SSE = \sum_{j=1}^{N_{obs}}\left(F_{x,exp,j}-F_{x,model,j}\right)^2 \tag{11}$$

Figure 5 shows the results of the fitting operation on the three tests in wet conditions with the rollers rotating at speeds of 100, 200 and 300 rpm, respectively. The graphs also show the value of the adhesion coefficient in wet conditions according to the theoretical model parameters suggested by Polach. The fitting operation on the forward curve in the 300-rpm test only considered creep values below 42% since the experimental data showed a clear adhesion recovery at this creepage value. The forward curve with creep values above 42% was not fitted due to the limited number of experimental records until wheel locking. In all tests, a hysteretic loop can be noticed, which means that two

separate adhesion curves are generated during the tests, corresponding to increasing (forward) and decreasing (backwards) creep rate, respectively. More in detail, the backwards curve shows higher values of adhesion with respect to the forward curve, however the hysteresis loop is more slender at lower roller speed values, since at a fixed creep value, the dissipated power, which is proportional to the sliding speed, is higher at larger values of speed. Moreover, at higher roller speed, the temperature at the contact patch is expected to grow, thus contributing to the removal of the water layer. However, the real temperature at the wheel-roller interface is extremely difficult to be directly measured on the bench.
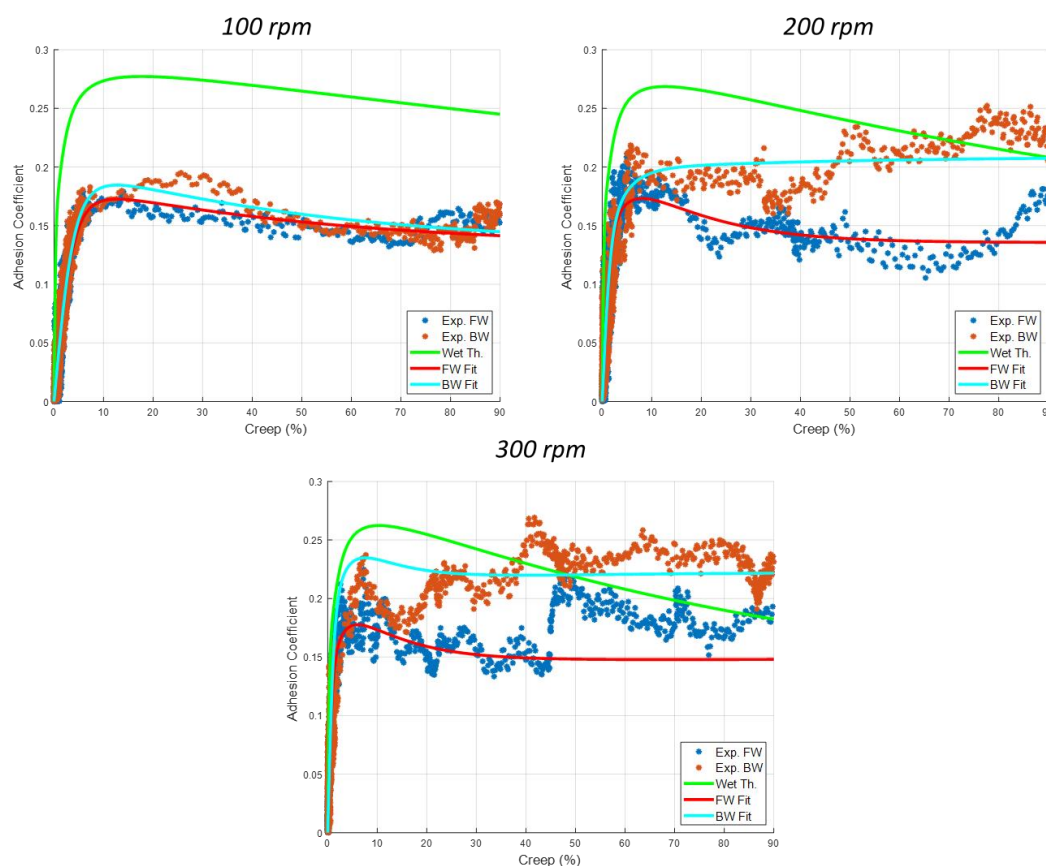

Figure 5. Fitting operation on the wheel adhesion recovery tests.

The values of the Polach model parameters obtained from the fitting operation are presented in Table 1, which also gives the theoretical values suggested by Polach for wet conditions. In the 100-rpm test, the μ_0 parameter is higher for the backwards curve, while the A and B parameters, related to the falling friction effect, have a limited variation, since the hysteresis loop is extremely slender. The forward and backwards curve have instead a similar value of the friction coefficient in the 200-rpm test, however the backward curve features larger values of the A and B parameter, meaning that the falling friction effect is reduced, due to the contaminant removal performed by the friction forces. Finally, the 300-rpm test shows the largest increase in the static friction coefficient, as well as higher values of the falling friction parameters for the backwards curve with respect to the forward one. For all fitting curves, the reduction factors of the linear and non-linear parts of the adhesion curve have extremely low values if compared to the theoretical parameters suggested by Polach. This is due to the fact that the maximum of the adhesion coefficient is obtained at creep values around 10% on the multi-axle scaled roller-rig even in dry conditions, while the theoretical models tend to predict creep values of about 1-2% when the maximum adhesion coefficient is attained. Such differences in the

initial slope of the adhesion curves obtained on roller-rigs were also found in [45,46,65]. Different possible reasons could explain these differences between the theoretical prediction and the experimental data collected on the multi-axle roller-rig. First, with the mechanical configuration of the new bench, the creepage values correspond to transient braking maneuvers, rather than to quasi-static operations. Furthermore, the Kalker's coefficient, which are a function of the material mechanical properties and of the semi-axes of the contact patch, could have an intrinsic scaling factor, which is not easy to account for. Moreover, roller-rigs feature large values of the spin creepage, while on real vehicles spin is negligible with respect to the longitudinal creepage during traction/braking operations. Finally, another source of disagreement could be the effect of the centrifugal force on the roller-rig, which has the effect to move the contaminant film away from the external surface of the rollers, thus drying them more quickly.

Table 1. Results of the fitting operation.

Parameter	Wet Th.	100 rpm		200 rpm		300 rpm	
		FW	BW	FW	BW	FW	BW
μ_0	0.3	0.19	0.21	0.25	0.25	0.24	0.34
A	0.4	0.69	0.64	0.56	0.85	0.62	0.67
B (s/m)	0.2	1	1	1.64	2.5	1.55	2
k_A	0.3	0.02	0.02	0.05	0.05	0.09	0.09
k_S	0.1	0.02	0.02	0.03	0.03	0.05	0.05

Despite these aspects, which will surely be addressed in future works, the multi-axle roller rig proves to be a suitable solution for the simulation of the wheel adhesion recovery phenomenon in laboratory conditions. Moreover, the curve fitting operation on the experimental data with the Polach model shows that due to the adhesion recovery phenomenon, the static friction coefficient and the parameters related to the falling friction effect tend to increase in the backwards curve because of the removal of the water contaminant lying on the roller surface, performed by the work of the friction forces at high creep values.

4.2. Rail adhesion recovery tests

As previously shown, the multi-axle roller-rig also allows to simulate the rail adhesion recovery phenomenon, which deals with the restoring of higher adhesion values on the trailing wheelsets of the vehicle, thanks to the cleaning effect performed by the leading axles running at high creep values.

A preliminary rail adhesion recovery phenomenon was performed on the multi-axle roller-rig by adjusting the axle-load on each wheelset to 785 N, corresponding to a full-vehicle axle-load of 10 ton. Low values of axle-loads were tested to reduce the wear rate of the wheel and roller rims. The test was performed with a roller speed equal to 390 rpm, to reproduce a full-scale speed of approximately 60 km/h. The test was carried out with three manual contamination of the roller-surface by pressing a wet sheet against the rotating surface of the rollers. Figure 6 shows a detailed view of the creepage values on each wheelset during the third contamination. The experimental results are in good agreement with the theoretical expectations. In fact, the first wheelset reaches the highest value of creepage and it is the last one to recover back to good adhesion conditions. On the other hand, the fourth wheelset features a limited increase of the creepage value during the contamination, since the other axles, reaching higher values of creepage, have a cleaning effect on the roller surfaces. A little anomaly can be noticed for wheelsets 2 and 3, since during the contamination, the third wheelset attains a higher creepage value with respect to the second axle. However, this could be due to little differences in the adhesion conditions of the rollers, to vibrations and little inefficiencies in the suspension systems. Nevertheless, good adhesion levels are restored first on the third axle and then on the second one, as expected. Therefore, the anomaly at the beginning of the contamination could be also due to the contamination process itself, which at this stage is carried out manually and could be non-uniform.
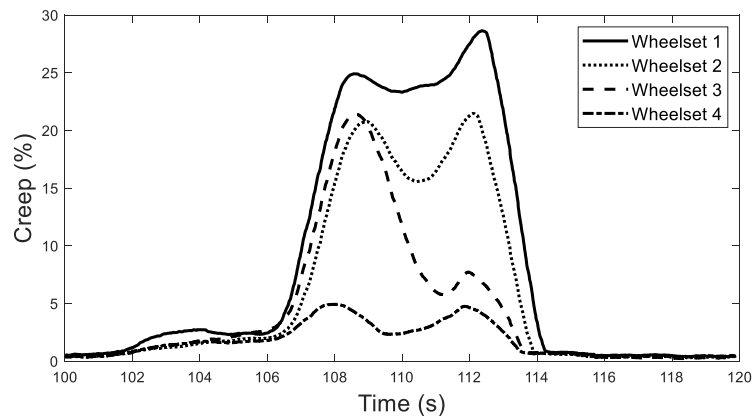
Figure 6. Rail adhesion recovery test.

5. Conclusions

The paper deals with the description of the mechanical and sensor arrangement of a new innovative multi-axle roller-rig, consisting of four scaled railway wheelsets rotating over a pair of powered rollers. The bench configuration was designed with the aim to simulate in laboratory conditions the adhesion recovery phenomena experienced in degraded adhesion conditions when large creep values are attained, and a cleaning effect is produced on both the rails and the wheels. In fact, these phenomena are difficult to investigate with on track-tests or by means of typical laboratory devices and therefore a new roller-rig configuration was required. The bench allows to simulate creepage values corresponding to transient braking operations, thanks to a pneumatic braking system which guarantees an independent braking effort on each of the four wheelsets. The bench allows for the simulation of three different types of tests, namely adhesion curve tests, wheel adhesion recovery tests and rail adhesion recovery tests.

Three wheel adhesion recovery tests were performed on wet roller surfaces with the rollers rotating at 100, 200 and 300 rpm respectively. The experimental data highlighted that when a contaminant is lying on the roller surface, a hysteresis loop is generated in the adhesion curve, i.e., the adhesion value at fixed creep depends on the sign of the creep time derivative. More in detail, when large creep values are attained, the work of the friction forces destroys part of the contaminant film and higher adhesion values can be reached. A fitting operation was performed on the experimental data with the Polach model. This operation showed that due to the cleaning effect of the friction forces, the backwards curve is described by higher values of the static friction coefficient and of the falling friction parameters in Polach equations. However, the fitting routine also pointed out that the slope of the adhesion curve is far lower with respect to the theoretical values suggested by Polach, due to the fact that on the roller-rig, the maximum of the adhesion coefficient is found at around 10% creep even in dry conditions. This can be due to the transient nature of the performed tests, to the high values of spin creepage on the roller-rig, to a scaling factor hidden in the Kalker's coefficients and to the effect of the centrifugal force (in case of degraded adhesion). Future works will deal with the investigation of this difference between scaled rigs and full vehicles.

A rail adhesion recovery test was also performed on the rig with discrete manual contaminations of the roller surfaces while applying a constant braking pressure on all four wheels, and the experimental results were in good agreement with the theoretical expectations. In future developments, an automatic contamination process will be designed to control the quantity of the contaminant applied at the interface.

References

[1]   Beagley TM and Pritchard C 1975 Wheel/rail adhesion - the overriding influence of water *Wear* **35** 299-313

[2]   Chen H, Ban T, Ishida M and Nakahara T 2002 Adhesion between rail/wheel under water lubricated contact *Wear* **253** 75-81

[3]   Chen H, Ban T, Ishida M and Nakahara T 2008 Experimental investigation of influential factors on adhesion between wheel and rail under wet conditions *Wear* **265** 1504-11

[4]   Cann PM 2006 The "leaves on the line" problem - A study of leaf residue film formation and lubricity under laboratory test conditions *Tribol. Lett.* **24** 151-8

[5]   Zhu Y, Olofsson U and Nilsson R 2014 A field test study of leaf contamination on railhead surfaces *Proc. Inst. Mech. Eng. F* **228** 71-84

[6]   Ishizaka K, Lewis SR and Lewis R 2017 The low adhesion problem due to leaf contamination in the wheel/rail contact: Bonding and low adhesion mechanisms *Wear* **378-379** 183-97

[7]   Zhu Y, Yang H and Wang W 2015 Twin-disc tests of iron oxides in dry and wet wheel−rail contacts *Proc. Inst. Mech. Eng. F* **230** 1066-76

[8]   Zhu Y 2017 The influence of iron oxides on wheel–rail contact: A literature review *Proc. Inst. Mech. Eng. F* **232** 734-43

[9]   Lewis R and Dwyer-Joyce RS 2006 Wear at the wheel/rail interface when sanding is used to increase adhesion *Proc. Inst. Mech. Eng. F* **220** 29-41

[10]   Arias-Cuevas O, Li Z and Lewis R 2011 A laboratory investigation on the influence of the particle size and slip during sanding on the adhesion and wear in the wheel-rail contact *Wear* **271** 14-24

[11]   Arias-Cuevas O, Li Z and Lewis R 2010 Investigating the lubricity and electrical insulation caused by sanding in dry wheel-rail contacts *Tribol. Lett.* **37** 623-35

[12]   Omasta M, Machatka M, Smejkal D, Hartl M and Křupka I 2015 Influence of sanding parameters on adhesion recovery in contaminated wheel-rail contact *Wear* **322-323** 218-25

[13]   Skipper WA, Chalisey A and Lewis R 2018 A review of railway sanding system research: adhesion restoration and leaf layer removal *Tribol. Mater. Surface Interfaces* **12** 237-51

[14]   Kalousek J and Magel E 1997 Modifying and managing friction *Railw. Track Struct.* **93**

[15]   Matsumoto A, Sato Y, Ono H, Wang Y, Yamamoto M, Tanimoto M and Oka Y 2002 Creep force characteristics between rail and wheel on scaled model *Wear* **253** 199-203

[16]   Li Z, Arias-Cuevas O, Lewis R and Gallardo-Hernández EA 2009 Rolling-sliding laboratory tests of friction modifiers in leaf contaminated wheel-rail contacts *Tribol. Lett.* **33** 97-109

[17]   Arias-Cuevas O, Li Z, Lewis R and Gallardo-Hernández EA 2010 Rolling-sliding laboratory tests of friction modifiers in dry and wet wheel-rail contacts *Wear* **268** 543-51

[18]   Galas R, Omasta M, Krupka I and Hartl M 2016 Laboratory investigation of ability of oil-based friction modifiers to control adhesion at wheel-rail interface *Wear* **368-369** 230-8

[19]   Harmon M and Lewis R 2016 Review of top of rail friction modifier tribology *Tribol. Mater. Surface Interfaces* **10** 150-62

[20]   Beagley TM, McEwen IJ and Pritchard C 1975 Wheel/rail adhesion-Boundary lubrication by oily fluids *Wear* **31** 77-88

[21]   Lewis SR, Lewis R, Evans G and Buckley-Johnstone LE 2012 Assessment of railway grease performance using a twin-disc tester *9th International Conference on Contact Mechanics and Wear of Rail/Wheel Systems, CM 2012*

[22]   Stützle T, Viereck U, Stribersky A, Rulka W, Enning M and Abel D 2006 Creepage control for use in wheelslide protection systems *11th IFAC Symposium on Control in Transportation Systems*

[23]   Nakazawa SI and Hijikata D 2017 Wheel slide protection system by the use of the tangential force in the macro slip area *Q. Rep. RTRI* **58** 196-203

[24]   Kondo K 2012 Anti-slip control technologies for the railway vehicle traction *2012 IEEE Vehicle Power and Propulsion Conference, VPPC 2012*

[25]   Pichlík P and Zdenek J 2014 Overview of slip control methods used in locomotives *Trans. Electr. Eng. Electron. Commun.* **2** 38-43

[26]   Zhao K, Li P, Zhang C, He J, Li Y and Yin T 2018 Online Accurate Estimation of the Wheel-Rail Adhesion Coefficient and Optimal Adhesion Antiskid Control of Heavy-Haul Electric Locomotives Based on Asymmetric Barrier Lyapunov Function *J. Sensors*

[27]   Nakazawa SI 2011 Development of a new wheel slide protection system using a new detection algorithm *Q. Rep. RTRI* **52** 136-40

[28]   Bosso N, Gugliotta A and Zampieri N 2012 RTCONTACT: An efficient wheel-rail contact algorithm for real-time dynamic simulations *2012 Joint Rail Conference, JRC 2012*

[29]   Kalker JJ and Johnson KL 1993 Three-Dimensional Elastic Bodies in Rolling Contact *J. Appl. Mech.* **60**

[30]   Kalker JJ 1982 A Fast Algorithm for the Simplified Theory of Rolling Contact *Veh. Syst. Dyn.* **11** 1-13

[31]   Shen ZY, Hedrick JK and Elkins JA 1983 A Comparison of Alternative Creep Force Models for Rail Vehicle Dynamic Analysis *Veh. Syst. Dyn.* **12** 79-83

[32]   Polach O 2000 A fast wheel-rail forces calculation computer code *Veh. Syst. Dyn.* **33** 728-39

[33]   Polach O 2005 Creep forces in simulations of traction vehicles running on adhesion limit *Wear* **258** 992-1000

[34]   Bosso N and Zampieri N 2018 A Novel Analytical Method to Calculate Wheel-Rail Tangential Forces and Validation on a Scaled Roller-Rig *Adv. Tribol.* **2018**

[35]   Vollebregt EAH 2014 Numerical modeling of measured railway creep versus creep-force curves with CONTACT *Wear* **314** 87-95

[36]   Spiryagin M, Polach O and Cole C 2013 Creep force modelling for rail traction vehicles based on the Fastsim algorithm *Veh. Syst. Dyn.* **51** 1765-83

[37]   Bosso N and Zampieri N 2020 Numerical stability of co-simulation approaches to evaluate wheel profile evolution due to wear *Int. J. Rail Transp.* **8** 159-79

[38]   Ridolfi A, Allotta B, Malvezzi M, Meli E, Pugi L, Rindi A and Vettori G 2012 Simulation of Railway Braking Tests under Degraded Adhesion Conditions *The 2nd Joint International Conference on Multibody System Dynamics (IMSD 2012)*

[39]   Allotta B, Meli E, Ridolfi A and Rindi A 2014 Development of an innovative wheel-rail contact model for the analysis of degraded adhesion in railway systems *Tribol. Int.* **69** 128-40

[40]   Meacci M, Shi Z, Butini E, Marini L, Meli E and Rindi A 2020 A railway local degraded adhesion model including variable friction, energy dissipation and adhesion recovery *Veh. Syst. Dyn.*

[41]   Bosso N, Gugliotta A, Magelli M, Oresta IF and Zampieri N 2019 Study of wheel-rail adhesion during braking maneuvers *Proc. Struct. Integrity* **24** 680-91

[42]   Gallardo-Hernandez EA and Lewis R 2008 Twin disc assessment of wheel/rail adhesion *Wear* **265** 1309-16

[43]   Zeng D, Lu L, Li Z, Zhang J, Jin X and Zhu M 2014 Influence of laser dispersed treatment on rolling contact wear and fatigue behavior of railway wheel steel *Mater. Des.* **54** 137-43

[44]   Jaschinski A, Chollet H, Iwnicki S, Wickens A and Von Würzen J 1999 The application of roller rigs to railway vehicle dynamics *Veh. Syst. Dyn.* **31** 345-92

[45]   Bosso N and Zampieri N 2013 Real-time implementation of a traction control algorithm on a scaled roller rig *Veh. Syst. Dyn.* **51** 517-41

[46]   Bosso N and Zampieri N 2014 Experimental and numerical simulation of wheel-rail adhesion and wear using a scaled roller rig and a real-time contact code *Shock. Vib.*

[47]   Bosso N, Gugliotta A and Zampieri N 2014 Study of adhesion and evaluation of the friction forces using a scaled roller-rig *5th World Tribology Congress, WTC 2013*

[48] Bosso N, Allen PD and Zampieri N 2019 Scale testing theory and approaches *Handbook of Railway Vehicle Dynamics, Second Edition*, ed Iwnicki S, Spiryagin M, Cole C and McSweeney T (Boca Raton: CRC Press/Taylor & Francis Group) pp. 825-67

[49] Bosso N, Soma A and Gugliotta A 2002 Introduction of a wheel-rail and wheel-roller contact model for independent wheels in a multibody code *ASME/IEEE Joint Railroad Conference*

[50] Bosso N, Gugliotta A and Somà A 2004 Dynamic Behavior of a Railway Wheelset on a Roller Rig versus Tangent Track *Shock. Vib.* **11** 280673

[51] Liu B and Bruni S 2015 Analysis of Wheel-Roller Contact and Comparison with the Wheel-Rail Case *Urban Rail Transit* **1** 215-26

[52] Voltr P and Lata M 2012 Masuring of wheel-rail adhesion characteristics at a test stand *18th International Conference Engineering Mechanics 2012*

[53] Voltr P and Lata M 2015 Transient wheel-rail adhesion characteristics under the cleaning effect of sliding *Veh. Syst. Dyn.* **53** 605-18

[54] Bosso N, Gugliotta A and Zampieri N 2015 Strategies to simulate wheel-rail adhesion in degraded conditions using a roller-rig *Veh. Syst. Dyn.* **53** 619-34

[55] Bosso N, Gugliotta A and Zampieri N 2016 A test rig for multi-wheelset adhesion experiments *Civil-Comp Proceedings* **110**

[56] Bosso N, Gugliotta A and Zampieri N 2018 Study of the wheel-rail adhesion under degraded conditions using a multi-axles roller-rig *The Dynamics of Vehicles on Roads and Tracks* **2** 803-8

[57] Bosso N, Gugliotta A, Magelli M and Zampieri N 2019 Experimental Setup of an Innovative Multi-Axle Roller Rig for the Investigation of the Adhesion Recovery Phenomenon *Exp. Tech.* **43** 695-706

[58] Jaschinski A 1991 On the application of similarity laws to a scaled railway bogie model (Doctoral Thesis) TU Delft

[59] Zampieri N, Bosso N and Gugliotta A 2016 Innovative monitoring systems for onboard vehicle diagnostics *Civil-Comp Proceedings*

[60] Bosso N, Magelli M and Zampieri N 2020 Calibration and development of a roller bench multi-axis for monitoring the braking system of a railway vehicle *Preprint Ingeneria Ferroviaria*

[61] Bosso N, Gugliotta A and Somà A 2006 Design and simulation of railway vehicles braking operation using a scaled roller-rig *WIT Transactions on the Built Environment* **88** 869-83

[62] Bosso N, Magelli M and Zampieri N 2019 Investigation of adhesion recovery phenomenon using a scaled roller-rig *Veh. Syst. Dyn.*

[63] Byrd RH, Hribar ME and Nocedal J 1999 An Interior Point Algorithm for Large-Scale Nonlinear Programming *SIAM J. Optim.* **9** 877-900

[64] Byrd RH, Gilbert JC and Nocedal J 2000 A trust region method based on interior point techniques for nonlinear programming *Math. Program.* **89** 149-85

[65] Fletcher DI and Lewis S 2013 Creep curve measurement to support wear and adhesion modelling, using a continuously variable creep twin disc machine *Wear* **298-299** 57-65